

# Causality by Abstraction: Symbolic Rule Learning in Multivariate Timeseries with Large Language Models

**Preetom Biswas**

*Arizona State University, Tempe, AZ, USA*

PBISWA11@ASU.EDU

**Giulia Pedrielli**

*Arizona State University, Tempe, AZ, USA*

GPEDRIEL@ASU.EDU

**K. Selçuk Candan**

*Arizona State University, Tempe, AZ, USA*

CANDAN@ASU.EDU

## Abstract

Inferring causal relations in timeseries data with delayed effects is a fundamental challenge, especially when the underlying system exhibits complex dynamics that cannot be captured by simple functional mappings. Traditional approaches often fail to produce generalized and interpretable explanations, as multiple distinct input trajectories may yield nearly indistinguishable outputs. In this work, we present `ruleXplain`, a framework that leverages Large Language Models (LLMs) to extract formal explanations for input-output relations in simulation-driven dynamical systems. Our method introduces a constrained symbolic rule language with temporal operators and delay semantics, enabling LLMs to generate verifiable causal rules through structured prompting. `ruleXplain` relies on the availability of a principled model (e.g., a simulator) that maps multivariate input time series to output time series. Within `ruleXplain`, the simulator is used to generate diverse counterfactual input trajectories that yield the same or closely matching target output, serving as candidate explanations. Such counterfactual inputs are clustered and provided as context to the LLM, which is tasked with the generation of symbolic rules encoding the joint temporal trends responsible for the patterns observable in the output times series. A closed-loop refinement process ensures rule consistency and semantic validity. We validate the framework using the `PySIRTEM` epidemic simulator, mapping testing rate inputs to daily infection counts; and the `EnergyPlus` building energy simulator, observing temperature and solar irradiance inputs to electricity needs. For validation, we perform three classes of experiments: (1) we verify the efficacy of the ruleset through input reconstruction; (2) we conduct ablation studies evaluating the causal encoding of the ruleset; and (3) we perform generalization tests of the extracted rules across unseen output trajectories with varying phase dynamics. The code is available [here](#).

**Keywords:** Causal inference, Timeseries analysis, Rule-Based Explanations, Large Language Models (LLMs), Closed-Loop Learning.

## 1. Introduction and Related Literature

Many scientific and engineering domains rely on high-fidelity physics-based simulators that model complex dynamical systems such as epidemic spread, climate projections, and autonomous driving testing. These simulators can accurately generate output timeseries from given inputs, yet they are typically treated as black boxes due to the inner complexity. While they reproduce dynamics, they do not provide transparent explanations of how qualitative behaviors in the output arise from patterns in the input. Timeseries data exacerbate such challenges due to temporal dependencies, delayed effects, high-dimensionality, and feedback loops, further complicating the characterization

of causal dependency. Approaches such as Granger causality (Granger, 1969), conditional independence methods (Chu et al., 2008; Runge, 2020), and Structural Equation Models (Peters et al., 2013) identify statistical dependencies over the complete simulation horizon. While insightful, these methods typically quantify aggregate influence rather than providing explicit relations between specific input trends and delayed qualitative output behaviors. These challenges are further complicated when both inputs and outputs are multivariate timeseries produced by a simulator whose structural equations are inaccessible (or intractable).

More recently, Large Language Models (LLMs) have gained prominence in this field due to their pattern recognition, explainable abstraction, and high reasoning capabilities. The attention mechanism in transformers-based LLMs can capture long-range dependencies and complex sequential patterns present in timeseries data (Abdullahi et al., 2025; Ekambaram et al., 2025). LLM architectures have accelerated timeseries forecasting by managing larger, more complex datasets and capturing non-linearities and dependencies directly from historical data (Liu et al., 2022, 2017, 2024). For example, Wang et al. (2025) combined numerical timeseries and text-based news inputs with chain-of-thought reasoning to connect events with temporal shifts. Also relevant, (Jin et al., 2024) introduce a framework that reprograms LLMs for timeseries forecasting by mapping timeseries into text-based representations, allowing few-shot and zero-shot prompting without modifying the pre-trained model. Other contributions have explored the construction of causal graphs to predict multi-variate timeseries progression (Orang et al., 2025). Despite such significant strides, few studies have proposed methodologies that attempt identifying generalized, explainable causal relations, especially between multi-variate timeseries inputs and outputs.

In this paper, we propose `ruleXplain`, a framework that leverages LLMs to infer generalizable, symbolic causal relations between multivariate input and output timeseries with delayed effects. Inspired by in-context learning (ICL) (Brown et al., 2020), our approach avoids fine-tuning by providing the LLM with a relevant set of input trajectories, i.e., diverse counterfactual inputs that yield similar output behaviors in a simulator. The LLM is prompted to synthesize a formal ruleset using a constrained symbolic language that captures conjunctions of input trends over time windows and their delayed implications on output phases (e.g., peak onset or plateau formation). These rules are iteratively refined in a closed-loop process: the LLM generates new input configurations based on the extracted rules, the simulator evaluates the resulting outputs, and the ruleset is adjusted to correct inconsistencies or refine the temporal window associated with each phase. The LLM is instructed to provide symbolic justifications for its decisions, akin to chain-of-thought prompting, but grounded in a formal logical schema. Finally, we evaluate the inference and generalizability of the extracted rules by testing their ability to generate plausible inputs for unseen output trajectories with distinct phase dynamics, validating the causal structure encoding capabilities of `ruleXplain`.

To demonstrate the framework, we use timeseries generated from the epidemiological simulator `PySIRTEM` (Biswas et al., 2025), studying the relationship between testing rates and daily infection trends, and the `EnergyPlus` simulator (Crawley et al., 2001), inferring causation between temperature and solar irradiance inputs and electricity consumption for a Supermarket System. Importantly, `ruleXplain` only uses raw numerical input-output timeseries without any specific semantics associated with epidemics, governing domain-specific dynamics, or underlying system information.

**Contributions.** `ruleXplain` introduces a symbolic and phase-aware framework for explainable causal inference in black-box timeseries systems. Specifically:

- (C1) **Symbolic framing of delayed causal inference:** We formalize timeseries causal inference as a symbolic rule identification task, introducing a constrained rule language with temporal operators and delay semantics. This shifts the focus from traditional forecasting or graph reconstruction toward interpretable, phase-based reasoning.
- (C2) **Domain-agnostic extraction from black-box simulators:** Our method infers interpretable causal abstractions without access to simulator equations or domain priors. It treats multivariate input-output timeseries purely as abstract signals, enabling general-purpose causal rule extraction across black-box systems.
- (C3) **LLM-in-the-loop rule synthesis:** We propose a novel prompting and refinement strategy that uses LLMs to generate, verify, and iteratively improve formal rulesets using a closed-loop process grounded in simulation feedback.
- (C4) **Generalization via input reconstruction:** We validate inference ability by reconstructing inputs for unseen output trajectories with distinct qualitative dynamics.

## 2. Methodology

Fig. 1 summarizes the ruleXplain pipeline.

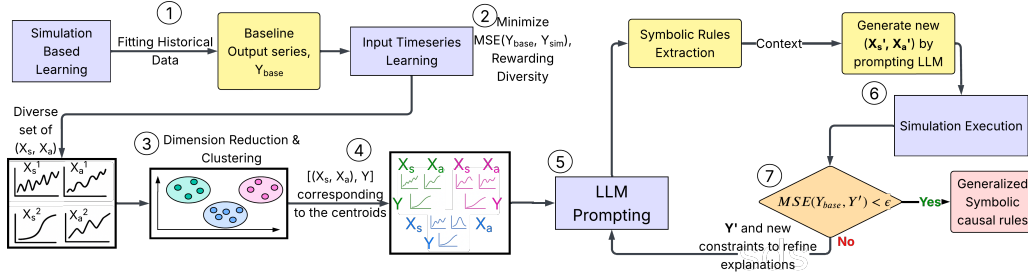


Figure 1: ruleXplain method overview key modules and interactions.

Executing the simulation for a given input, we obtain a baseline output trajectory  $Y_{base}$ . A learning module then generates diverse multivariate input timeseries that fit  $Y_{base}$ . These diverse input-output pairs form the basis for extracting causal structure (Sec. 2.1).

To reduce redundancy, we apply dimensionality reduction and clustering to select representative input-output trajectories (Sec. 2.2). The resulting cluster centroids are used as context for the LLM, which generates a symbolic ruleset  $\mathcal{R}$  capturing temporal input trends and their delayed effects on output phases (Sec. 2.3).

Next, the LLM generates new input timeseries consistent with  $\mathcal{R}$ , which are evaluated through the simulator to produce an output  $Y'$ . The validity of  $\mathcal{R}$  is assessed by comparing  $Y'$  with  $Y_{base}$ . If the deviation exceeds a threshold  $\epsilon$ , the mismatch is used as feedback to refine  $\mathcal{R}$  in a closed-loop manner. This iterative process enforces the logical constraints until the ruleset  $\mathcal{R}$  yields inputs that produce output trajectories within acceptable deviation from  $Y_{base}$  (Sec. 2.3).

### 2.1. Input Timeseries Learning Module

Given a *Baseline Output* trajectory  $Y_{base}$  of length  $T$ , the goal of the learning module is to construct diverse inputs (as multivariate time series)  $X_t$  that would result in similar output  $Y_{sim} \approx Y_{base}$ .

We sequentially generate a set of  $N$  diverse input time series,  $\mathcal{A}_N = \{\mathbf{X}_t^p\}_{p=1}^N$  that minimize deviation from the baseline output while maintaining diversity among previously discovered solutions. Here, each component of the input is a time series, i.e.,  $X_j = \{x_{j,1}, x_{j,2}, \dots, x_{j,T}\}$  for each component  $j = 1, \dots, J$ . For each iteration  $p = 1, \dots, N$ , we solve:

$$P_{\text{LEARN}}(p) : \min_{\mathbf{X}^p} L_{\text{out}}(Y_{\text{sim}}(\mathbf{X}^p), Y_{\text{base}}) - \lambda_{\text{arch}} D_{\text{arch}}(\mathbf{X}^p, \mathcal{A}_{p-1}) \quad (1)$$

$$\text{s.t. } \ell_{j,t} \leq x_{j,t}^p \leq u_{j,t}, \quad \forall j = 1 \dots, J \text{ and } t \in \{1, \dots, T\}.$$

In problem  $P_{\text{LEARN}}(p)$ , we have:

$$L_{\text{out}}(\cdot) = \frac{1}{T} \sum_{t=1}^T (Y_{\text{sim},t}(\mathbf{X}_t^p) - Y_{\text{base},t})^2; \quad D_{\text{arch}}(\cdot) = \frac{1}{|\mathcal{A}_{p-1}|} \sum_{\ell=1}^{|\mathcal{A}_{p-1}|} d^\ell,$$

$$\text{where: } d^\ell = \sum_{j=1}^J \left\{ \frac{1}{T} \sum_{t=1}^T \left| \frac{x_{j,t}^p - x_{j,t}^\ell}{x_{j,t}^\ell} \right| \right\}.$$

Solving  $P_{\text{LEARN}}(p)$  sequentially for  $p = 1, \dots, N$  yields a set of *diverse* input time series  $\{(\mathbf{X}_t^p)_{t=1}^T\}_{p=1}^N$  that produce a similar baseline trajectory  $Y_{\text{base}}$  (the cost  $L_{\text{out}}$ ). To enforce diversity, we maintain an archive  $\mathcal{A}$  of previously generated solutions. At iteration  $p$ , the archive  $\mathcal{A}_{p-1}$  contains all time series  $\{(\mathbf{X}_t^i)_{t=1}^T\}_{i=1}^{p-1}$ , with  $\mathcal{A}_0 = \emptyset$ , and the newly obtained solution is added after each iteration. The diversity term  $D_{\text{arch}}$  quantifies the sum of the average difference between the candidate input ( $\mathbf{X}_t^p$ ) and each archived input across all time steps and input components, weighted by  $\lambda_{\text{arch}}$  which is chosen by the user to balance diversity.

To incrementally solve  $P_{\text{LEARN}}(p)$ ,  $p = 1, \dots, N$  we employed the Tree-structured Parzen Estimator (TPE) algorithm (Watanabe, 2023) in the Optuna environment (Akiba et al., 2019).

## 2.2. Dimensionality Reduction and Clustering

To form the training set for the explanation generation step, we apply dimensionality reduction and clustering on the set of timeseries resulting from the learning step (Sec. 2.1),  $\{(\mathbf{X}_t^p)_{t=1}^T\}_{p=1}^N$ .

Specifically, we employ the Uniform Manifold Approximation and Projection (UMAP) (McInnes et al., 2020) technique to represent the data points in a 2-D space embedding and partition into clusters through  $K$ -Means clustering, from which a single centroid representative  $(\mathbf{X}_t^c)_{t=1}^T$  is selected per cluster. The resulting input-output pairs  $\{(\mathbf{X}_t^c)_{t=1}^T, Y_{\text{sim}}^c\}$  serve as the training context for the LLM during explanation generation (Sec. 2.3).

This reduction step preserves diversity while eliminating redundant examples that could bias the learned ruleset toward over-specific patterns. Implementation details are provided in Appendix A.3.

## 2.3. LLM-based Explanation Generation

The explanation generation component of the proposed `ruleXplain` consists of two steps: (i) initial ruleset elicitation based on the cluster-derived context and (ii) closed-loop rule refinement process. The specific LLM used in this work is the OpenAI gpt4.1 (OpenAI, 2024). The complete procedure is also summarized in Table 1.

**Initial Explanation Inference.** This step receives as input the centroids resulting from the clustering (Sec. 2.2), namely  $\left(\mathbf{X}_t^p, Y_{\text{sim}}^c\right)$ , which we refer to as the *context*, for generating the initial set of explainable symbolic rules that characterize the relationship between input and output timeseries. Notably, we avoid providing `ruleXplain` with prior knowledge of the underlying system dynamics (e.g., epidemics-specific transmission dynamics) and domain-specific notations. Instead, variables are presented purely as abstract timeseries data without any explicit reference to their physical meaning and/or regulating equations, conveying only the existence of a causal relationship. Since  $Y_{\text{sim}}^c \approx Y_{\text{base}}$ , we will represent the contexts with  $\left\{\left(\mathbf{X}_t^c\right)_{t=1}^T, Y_{\text{base}}\right\}$ .

Along with the aforementioned context, through prompting, we further guide the LLM to infer a causal ruleset by stating the following general properties: (i) direct/inverse trend between  $\left(\mathbf{X}_t^c\right)_{t=1}^T$  and  $Y$ , without providing an indication of proportionality, (ii) delayed effect (temporal lag) between the input (cause) and the output series (effect) and, (iii) explicit constraints on structure, format, and vocabulary to ensure reproducibility and consistency (Sec. 2.3). The specific prompt to generate the initial set of rules is listed in Appendix C.

**Closed-loop Rule Refinement.** Given the initial ruleset, the closed-loop refinement pipeline iterates until an *acceptable* set of rules is obtained, i.e., when the input sequence generated from the ruleset yields an output  $Y_{\text{sim}}$  sufficiently similar to the baseline output. Without loss of generality, we say that two time series are similar when the distance measure  $L_{\text{out}}(Y_{\text{sim}}, Y_{\text{base}})$  is bounded by a user selected positive  $\epsilon$ . The refinement iterates through three key steps:

- i) **Input set generation using the initial ruleset.** Given the cluster-derived context, we prompt the LLM to generate a unique input timeseries  $\mathbf{X}' = (\mathbf{x}'_1, \dots, \mathbf{x}'_T)$  that differs from the cluster-derived inputs  $\left\{\left(\mathbf{X}_t^c\right)_{t=1}^T\right\}_{c=1}^C$  but remains strictly consistent with the initial ruleset. We prompt the LLM to identify the different phases, predefined by a schema, and generate the input configurations accordingly. Moreover, the LLM is instructed to justify the generated input values to prevent misalignment with the previously inferred relationships.
- ii) **Evaluation of the new input.** The generated input timeseries are evaluated by executing the simulator, obtaining the corresponding output trace  $Y'$ . All other simulator hyperparameters remain unmodified.
- iii) **Ruleset refinement.** The new input-output pair  $\left\{\left(\mathbf{X}'_t\right)_{t=1}^T, Y'\right\}$  is then returned to the LLM model along with the baseline  $Y_{\text{base}}$  to quantify the deviation  $L_{\text{out}}(Y_{\text{sim}}, Y_{\text{base}})$ . The LLM also retains the cluster contexts and prior iteration results. By evaluating the  $\left\{\left(\mathbf{X}'_t\right)_{t=1}^T, Y'\right\}$  and  $Y_{\text{base}}$ , the LLM identifies inaccurate symbolic rules and generates a *modified* (refined) ruleset. Additional qualitative constraints (such as “ $Y'$  displays weaker resurgence than  $Y_{\text{base}}$ ”, and “the inputs should not oscillate”) are provided as constraints to guide ruleset refinement. The rationale behind iterative refinement with progressive constraints, instead of offering all the constraints initially, is to reduce reasoning load and avoid overwhelming the model. At this stage of `ruleXplain` development, the constraints are added manually based on observed deviations in  $Y_{\text{base}}$  and  $Y'$ .

**Formal Representation of Extracted Rules** To formalize the structure of the extracted rules, we adopt a symbolic and temporal logic-based notation to describe causal dependencies between trends in the input timeseries and phases of the output. Each rule is represented as a temporal implication of the form:

$$\square_{[t_1, t_2]} (\text{Trend}_h(X_h) \wedge \text{Trend}_j(X_j)) \rightarrow \diamond_{[t_3, t_4]} \text{Phase}(Y) \quad (2)$$

where  $h$  and  $j$  are two particular dimensions of the input timeseries. Here:

- $\text{Trend}(X.)$  is a unary predicate applied to an input series over interval  $[t_1, t_2]$ , drawn from a fixed vocabulary  $\mathcal{T}$  (e.g., `Low`, `SharpSpike`, `HighStable`).
- $\text{Phase}(Y)$  is a qualitative output behavior over  $[t_3, t_4]$ , drawn from a vocabulary  $\mathcal{P}$  (e.g., `InitialGrowth`, `PeakFormation`).
- $\square$  and  $\diamond$  denote persistent and eventual satisfaction of input and output properties over their respective intervals.
- Rules may include explicit delay constraints:  $t_3 > t_2$ .
- The delay  $\delta = t_3 - t_2$  captures the temporal lag between cause and effect.

As an illustrative example, consider the rule:

$$\square_{[t_1, t_2]} (\text{SlowRise}(X_h) \wedge \text{Low}(X_j)) \rightarrow \diamond_{[t_3, t_4]} \text{PeakFormation}(Y) \quad (3)$$

This rule states that if  $X_h$  slowly rises and  $X_j$  remains low over a time window  $[t_1, t_2]$ , then a peak in  $Y$  will occur in the delayed interval  $[t_3, t_4]$ . The ruleset  $\mathcal{R}$  is composed of multiple such formulas, one per output phase, and provides an interpretable symbolic explanation of the causal dynamics.

Table 1: Stepwise process for Causal Rules Inference through LLM.

<b>Procedure: Explanation Generation and Refinement</b>
<b>Step 1: Initialize.</b> Extract an initial ruleset $R_0$ derived from Cluster-derived context $[(\mathbf{X}_t^c)_{t=1}^T, Y_{base}]_{c=1}^C$ pairs.
<b>Step 2: Generate Inputs.</b> Use $R_i$ and $[(\mathbf{X}_t^c)_{t=1}^T, Y_{base}]_{c=1}^C$ to prompt novel input sequences $(\mathbf{X}_t^{(i)})_{t=1}^T$ that approximately reproduce the baseline trajectory $Y_{base}$ .
<b>Step 3: Simulate &amp; Evaluate.</b> Run the simulator and compute deviation $\Delta^{(i)}$ using the loss $L_{out}$ calculated from $Y^{(i)}$ and $Y_{base}$ .
<b>Step 4: Update Rules.</b> If $\Delta^{(i)} > \epsilon$ , update $R_i$ based on observed mismatches and added constraints to get $R_{i+1}$ .
<b>Step 5: Repeat.</b> Continue Steps 2–4 until $\Delta^{(i)} \leq \epsilon$ or the maximum number of iterations is reached, yielding the refined ruleset $R_{final}$ . Please note that $[(\mathbf{X}_t^c)_{t=1}^T, Y_{base}]_{c=1}^C$ remain unchanged across iterations.

### 3. Numerical Experiments

In this section, through set of validation experiments, we address three questions:

- Q1. Do the rules generated within `ruleXplain` lead to increasingly more accurate and explainable timeseries?
- Q2. How much does the ruleset or context impact the quality of the generated input timeseries?
- Q3. Is the ruleset generalizable to any baseline timeseries?

#### 3.1. Simulation Environments

To demonstrate `ruleXplain`, we use different two simulation environments:

- `PySIRTEM` (Biswas et al., 2025). For this epidemic simulator, the relevant input-output pair for the causal analysis is  $\{(\mathbf{X}_t^p)_{t=1}^T, Y\} \equiv \{(X_{s,t}, X_{a,t}), Y\}$ , where  $X_s$  and  $X_a$  denote the symptomatic and asymptomatic testing-rate, respectively, and  $Y$  denotes the daily infected

cases over  $T = 100$  days. The input trajectories vary weekly, consistent with the simulator assumptions.

- EnergyPlus (Crawley et al., 2001). For this building energy simulator, the relevant input–output pair is  $(X_d, X_g), Y$ , where  $X_d$  denotes Dry Bulb Temperature ( $^{\circ}C$ ),  $X_g$  denotes solar input, i.e., the global horizontal irradiance ( $Wh/m^2$ ), and  $Y$  denotes building electricity usage ( $J$ ) for a supermarket setting. Inputs vary hourly and horizon is  $T = 100$  hours.

In our experiments, we treat the simulator as a black box: its internal equations and parameters remain fixed and are not used by ruleXplain. A detailed description of the PySIRTEM and EnergyPlus model dynamics is provided in Appendix A.1- A.2.

### 3.2. Q1: Evaluation of Ruleset-Generated Input Timeseries

To address Q1, we apply ruleXplain to extract symbolic rules describing the relationship between multivariate input time series and the target output trajectory. For each simulation environment, we first select a baseline output time series  $Y_{\text{base}}$  over a fixed horizon ( $T = 100$ ). For PySIRTEM, we used the daily infection data from March 22 to June 30, 2020 (CTW, n.d.) and for EnergyPlus, the electricity consumption for a supermarket setup in Miami, FL from Jan 1 to Jan 5, 1997. From the baseline output, we solved  $P_{\text{LEARN}}(p)$  for  $p = 1, \dots, N = 20$  obtaining a preliminary set  $\mathcal{A}$  with  $|\mathcal{A}| = 20$  top performing input timeseries  $\{(X_s^\ell, X_a^\ell)\}_{\ell=1}^{|\mathcal{A}|}$  ranked by distance measure from the baseline,  $L_{\text{out}}$ . The centroid timeseries  $\{(\mathbf{X}_t^c)_{t=1}^T\}_{c=1}^C$ , obtained from U-MAP projection and K-Means clustering, were used as input to the simulators (PySIRTEM and EnergyPlus) to produce the  $Y_{\text{sim}} \approx Y_{\text{base}}$ . Given the clusters (context)  $\{(\mathbf{X}_t^c)_{t=1}^T, Y_{\text{base}}\}$ , we can then execute the procedure detailed in Sec. 2.3, where we infer the formal rulesets  $\mathcal{R}_{\text{final}}$  for both PySIRTEM and EnergyPlus (complete rulesets are reported in Appendix B, Table 2- 3).

Fig. 2- 3 shows the input–output trajectories resulting from the final ruleset  $\mathcal{R}_{\text{final}}$  produced by ruleXplain, for both PySIRTEM and EnergyPlus respectively, along with centroid context timeseries. The close temporal and magnitude alignment of the simulated  $Y_{\text{final}}$  and  $Y_{\text{base}}$  is indicative of the accuracy and effectiveness of  $\mathcal{R}_{\text{final}}$  in explaining the inherent (and unknown) dynamics emerging from the principled simulation. In particular, for EnergyPlus, the periodic structure of the output signal is also effectively reflected through the inferred input patterns. Across all our experiments we consistently observed lower errors as a function of the ruleXplain iterates, thus supporting convergence of the proposed approach (numerical evidence is reported in Appendix B, Fig. 8).

### 3.3. Q2: Impact of Ruleset and Cluster-Derived Context

We examine how much causal information is encoded in the causal ruleset and the cluster-derived context by using them to generate input timeseries corresponding to a fixed target output  $Y_{\text{base}}$  in our PySIRTEM experiment. Specifically, we evaluate three scenarios: (S1) *no ruleset and no clustering context*, (S2) *ruleset only*, and (S3) *ruleset with clustering context*. This comparative setup allows us to isolate and quantify the contribution of  $\mathcal{R}_{\text{final}}$  and contextual examples to the accuracy and novelty of the generated inputs. The specific prompts for each experiment are listed in the Appendix C.2.

Fig. 4- 5 display a clear progressive improvement from S1 to S2. The no-guidance (S1) scenario produces outputs with the least accuracy, which is significantly increased with  $\mathcal{R}_{\text{final}}$  (S2). Adding clustering context (S3) yields mixed effects, reporting slight improvement for PySIRTEM, but less flexible to baseline trends for EnergyPlus. This suggests potential overfitting to the examples

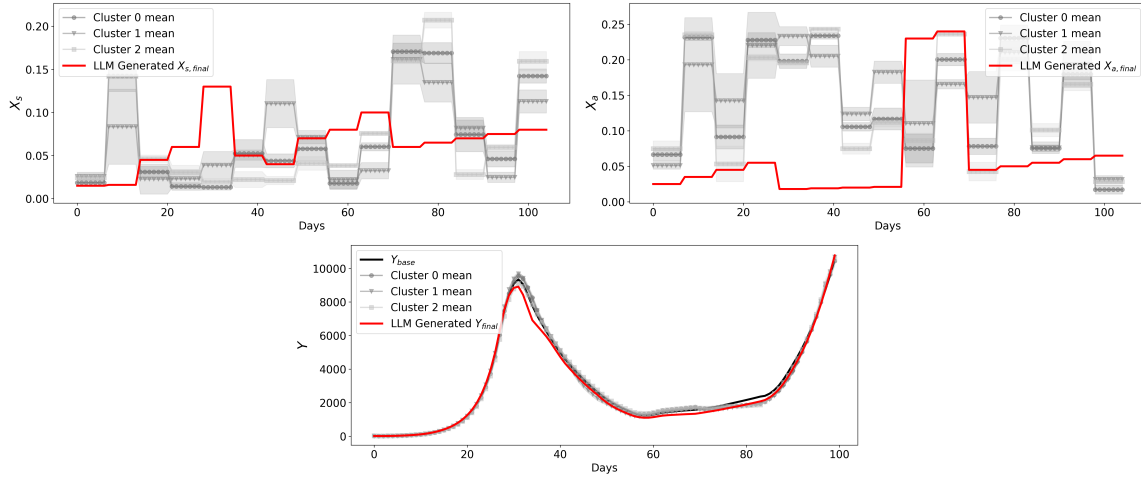


Figure 2: Timeseries  $X_s$ ,  $X_a$ , and  $Y$  generated using  $\mathcal{R}_{final}$  for PySIRTEM.

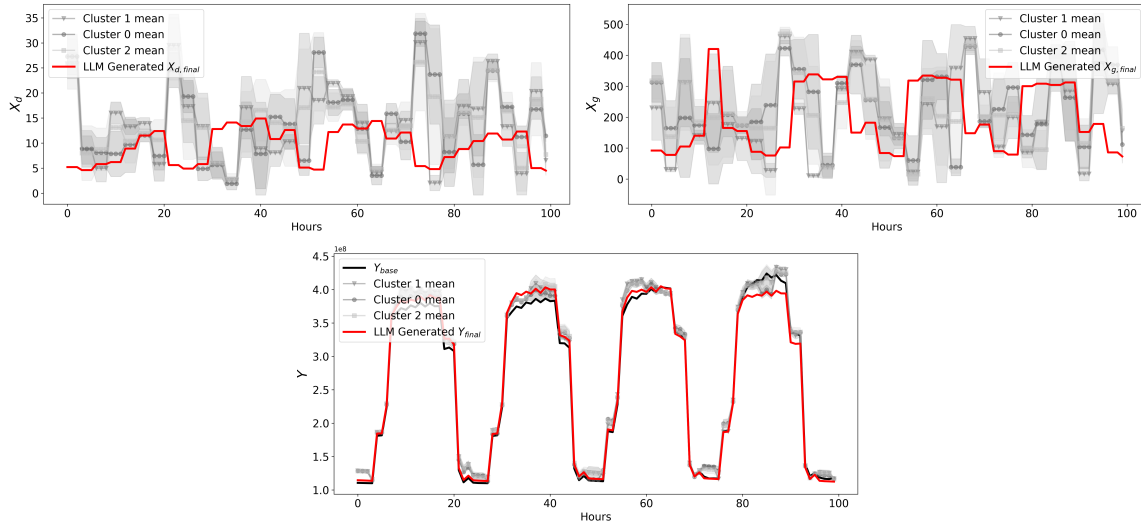
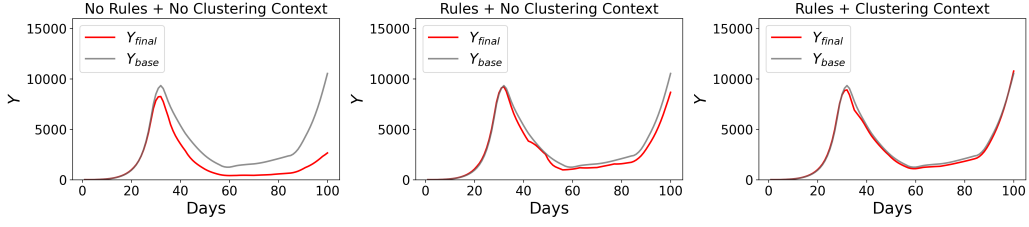
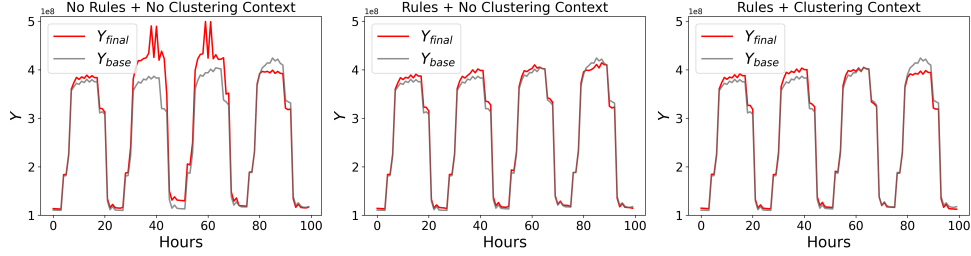


Figure 3: Timeseries  $X_d$ ,  $X_g$ , and  $Y$  generated using  $\mathcal{R}_{final}$  for EnergyPlus.

rather than improved adherence to the baseline and ruleset. The progression, particularly the major gain from S1 to S2, corroborate the encoding ability of causal information in the ruleXplain-generated ruleset, while addition of context in downstream tasks could overbias the model.

Across all scenarios, the timing of key phases (e.g. peak and decline) are aligned with  $Y_{base}$ . We conjecture it to be due to the underlying physics of system: specific parameters govern certain qualitative properties. For example, in PySIRTEM, infection rate is the primary driver of the disease progression which is kept constant to infer causal dependency between decidable human-regulated testing rates and corresponding infection case trends. Similarly, in EnergyPlus, we isolate the influence of observable weather inputs (e.g., temperature) on facility-level electricity consumption. In both cases, our focus was to generate interpretable insights that can support decision makers.


 Figure 4: Causal Encoding Comparison of  $\mathcal{R}_{\text{final}}$  through scenarios S1-S3 for PySIRTEM.

 Figure 5: Causal Encoding Comparison of  $\mathcal{R}_{\text{final}}$  through scenarios S1-S3 for EnergyPlus.

### 3.4. Q3: Results Generalizability Across Baselines

We assess whether the ruleset  $\mathcal{R}_{\text{final}}$  inferred from a specific baseline  $Y_{\text{base}}$  timeseries and cluster-derived contexts  $((X_s^c, X_a^c), Y_{\text{sim}}^c)$ , if utilized to construct input timeseries for a different  $Y'_{\text{base}}$ , produce a timeseries  $Y'_{\text{final}} \approx Y'_{\text{base}}$ . Due to space limitation, we perform this experiment only for our PySIRTEM setup where we varied testing and infection rates to produce two  $Y_{\text{base}}$  patterns with the following properties:

- i)  $Y_{\text{base}}^1$  with **prominent phase changes** that are easily mapped by the symbolic ruleset, but differing in timing (i.e., prolonged low initial phase, sharp peak no resurgence).
- ii)  $Y_{\text{base}}^2$  with **less distinct, non-prominent phase dynamics** that cannot be directly mapped to the ruleset (i.e. prolonged low initial phase, mild growth, slight dip, and late high resurgence).

For each baseline, we perform two experiments:

- (E1) We provide the LLM with the ruleset but no clustering context (see Sec. 3.3). The objective is to assess whether the ruleset inferred from another baseline *alone* can generate inputs  $(X_a, X_s)$  with acceptable accuracy for the new baselines  $Y_{\text{base}}^i$ ,  $i = 1, 2$ .
- (E2) We modify the ruleset by inverting and replacing a subset of causal relationships, producing an **inaccurate** ruleset  $\mathcal{R}_{\text{incorrect}}$ , (provided in Appendix C, Table 4). We then examine how rule inaccuracies affect input generation and the alignment between  $Y_{\text{incorrect}}$  and  $Y_{\text{base}}$ .

Fig. 6 demonstrates the ability of the  $\mathcal{R}_{\text{final}}$ -induced inputs to infer trajectories that produce accurate outputs under both prominent and non-prominent phase dynamics (Fig. 6). In both cases, inputs generated under  $\mathcal{R}_{\text{final}}$  capture the progression of  $Y_{\text{base}}$  with reasonable accuracy. In contrast, under the modified ruleset  $\mathcal{R}_{\text{incorrect}}$  we observe substantially greater misalignment—both temporally and in magnitude—between  $Y_{\text{incorrect}}$  and  $Y_{\text{base}}$ . This supports the importance of a well-defined, structured ruleset for improved input generation.

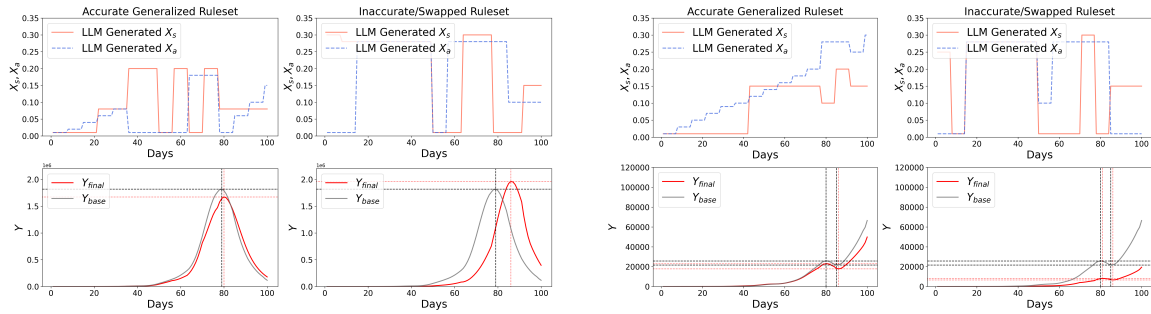


Figure 6: Input Inference for an alternate (left)  $Y_{base}^1$  with Prominent Phase Changes (right)  $Y_{base}^2$  with Non-Prominent Phase Changes. E1 results are in the left subplot, E2 in the right subplot for each.

**Discussion and limitations.** While our evaluations demonstrate that the extracted rules are syntactically valid, semantically consistent, and effective in generating novel inputs given outputs, we acknowledge several limitations. First, our framework does not aim to recover the “ground-truth” generative rules of the simulator, instead constructing symbolic rules within a constrained logical grammar that provide valid and reusable causal explanations for observed trajectories. As such, traditional accuracy-based comparisons against latent mechanistic models are not applicable. Secondly, we do not benchmark against existing symbolic rule learners or interpretable predictors (e.g., shapelet-based classifiers or symbolic regression), as our objective is not prediction or classification, but symbolic abstraction of delayed causal relations in high-dimensional temporal simulations.

#### 4. Conclusions and Future Work

We presented `ruleXplain`, a symbolic rule learning framework for causal abstraction in multivariate timeseries data. Unlike traditional forecasting or structural inference methods, `ruleXplain` constructs formal causal rules expressed in a constrained, human-interpretable symbolic language with explicit temporal and delay semantics. This structure enables LLMs to generate reusable explanations that link input trends to output phase behaviors without relying on domain-specific knowledge or direct simulator access. We demonstrate the approach across two distinct models and domains: an epidemic simulator mapping human-regulated testing rates to infection counts, and a building energy simulator mapping weather variables to electricity usage. Despite their differences in signal characteristics, periodicity, and causal structure, `ruleXplain` successfully extracts reusable symbolic rules that capture the governing temporal relationships. The closed-loop synthesis-and-verification process ensures rules are refined through simulation feedback, enabling robust alignment between symbolic explanations and system dynamics. We demonstrate the framework ability to generalize rules across diverse input trajectories and regenerate semantically consistent counterfactual inputs. The ruleset structured form makes it suitable for applications in counterfactual reasoning, treatment effect analysis, and simulation auditing.

Future work will explore adaptive clustering for more informative reference trajectories, fine-tuning LLMs for improved rule refinement, and agentic approaches to autonomously introduce logical constraints scalably and systematically. We also aim to develop hybrid evaluation metrics that balance fidelity, simplicity, and semantic alignment to benchmark symbolic causal frameworks like `ruleXplain` against emerging alternatives.

## References

- Shamsu Abdullahi, Kamaluddeen Usman Danyaro, Abubakar Zakari, Izzatdin Abdul Aziz, Noor Amila Wan Abdullah Zawawi, and Shamsuddeen Adamu. Time-series large language models: A systematic review of state-of-the-art. *IEEE Access*, 13:30235–30261, 2025. doi: 10.1109/ACCESS.2025.3535782.
- Takuya Akiba, Shotaro Sano, Toshihiko Yanase, Takeru Ohta, and Masanori Koyama. Op-tuna: A next-generation hyperparameter optimization framework. In *Proceedings of the 25th ACM SIGKDD International Conference on Knowledge Discovery & Data Mining, KDD '19*, page 2623–2631, New York, NY, USA, 2019. Association for Computing Machinery. ISBN 9781450362016. doi: 10.1145/3292500.3330701. URL <https://doi.org/10.1145/3292500.3330701>.
- Fahim Tasneema Azad, Robert W. Dodge, Allen M. Varghese, Jaejin Lee, Giulia Pedrielli, K. Selçuk Candan, and Gerardo Chowell-Puente. Sirtem: Spatially informed rapid testing for epidemic modeling and response to covid-19. *ACM Trans. Spatial Algorithms Syst.*, 8(4), November 2022. ISSN 2374-0353. doi: 10.1145/3555310. URL <https://doi.org/10.1145/3555310>.
- Preetom Biswas, Giulia Pedrielli, and K Selçuk Candan. Pysirtem: An efficient modular simulation platform for the analysis of pandemic scenarios. *medRxiv*, pages 2025–05, 2025.
- Tom B. Brown, Benjamin Mann, Nick Ryder, Melanie Subbiah, Jared Kaplan, Prafulla Dhariwal, Arvind Neelakantan, Pranav Shyam, Girish Sastry, Amanda Askell, Sandhini Agarwal, Ariel Herbert-Voss, Gretchen Krueger, Tom Henighan, Rewon Child, Aditya Ramesh, Daniel M. Ziegler, Jeffrey Wu, Clemens Winter, Christopher Hesse, Mark Chen, Eric Sigler, Mateusz Litwin, Scott Gray, Benjamin Chess, Jack Clark, Christopher Berner, Sam McCandlish, Alec Radford, Ilya Sutskever, and Dario Amodei. Language models are few-shot learners. In *Proceedings of the 34th International Conference on Neural Information Processing Systems, NIPS '20*, Red Hook, NY, USA, 2020. Curran Associates Inc. ISBN 9781713829546.
- Tianjiao Chu, Clark Glymour, and Greg Ridgeway. Search for additive nonlinear time series causal models. *Journal of Machine Learning Research*, 9(5), 2008.
- Drury B Crawley, Linda K Lawrie, Frederick C Winkelmann, Walter F Buhl, Y Joe Huang, Curtis O Pedersen, Richard K Strand, Richard J Liesen, Daniel E Fisher, Michael J Witte, et al. Energy-plus: creating a new-generation building energy simulation program. *Energy and buildings*, 33(4):319–331, 2001.
- CTW. The covid tracking project, n.d. Retrieved from <https://covidtracking.com/data>.
- Vijay Ekambaram, Arindam Jati, Pankaj Dayama, Sumanta Mukherjee, Nam H. Nguyen, Wesley M. Gifford, Chandra Reddy, and Jayant Kalagnanam. Tiny time mixers (ttms): fast pre-trained models for enhanced zero/few-shot forecasting of multivariate time series. In *Proceedings of the 38th International Conference on Neural Information Processing Systems, NIPS '24*, Red Hook, NY, USA, 2025. Curran Associates Inc. ISBN 9798331314385.
- Clive WJ Granger. Investigating causal relations by econometric models and cross-spectral methods. *Econometrica: journal of the Econometric Society*, pages 424–438, 1969.

- Ming Jin, Shiyu Wang, Lintao Ma, Zhixuan Chu, James Y. Zhang, Xiaoming Shi, Pin-Yu Chen, Yuxuan Liang, Yuan-Fang Li, Shirui Pan, and Qingsong Wen. Time-llm: Time series forecasting by reprogramming large language models, 2024. URL <https://arxiv.org/abs/2310.01728>.
- Chang Liu, Zhijian Jin, Jie Gu, and Caiming Qiu. Short-term load forecasting using a long short-term memory network. In *2017 IEEE PES Innovative Smart Grid Technologies Conference Europe (ISGT-Europe)*, pages 1–6, 2017. doi: 10.1109/ISGTEurope.2017.8260110.
- Chenxi Liu, Sun Yang, Qianxiang Xu, Zhishuai Li, Cheng Long, Ziyue Li, and Rui Zhao. Spatial-temporal large language model for traffic prediction, 2024. URL <https://arxiv.org/abs/2401.10134>.
- Shizhan Liu, Hang Yu, Cong Liao, Jianguo Li, Weiyao Lin, Alex X. Liu, and Schahram Dustdar. Pyraformer: Low-complexity pyramidal attention for long-range time series modeling and forecasting. In *International Conference on Learning Representations*, 2022. URL <https://openreview.net/forum?id=0EXmFzUn5I>.
- Leland McInnes, John Healy, and James Melville. Umap: Uniform manifold approximation and projection for dimension reduction. 2020. URL <https://arxiv.org/abs/1802.03426>.
- OpenAI. Gpt-4.1. <https://openai.com>, 2024. Accessed: 2025-07-29.
- Omid Orang, Patricia O. Lucas, Gabriel I. F. Paiva, Petronio C. L. Silva, Felipe Augusto Rocha da Silva, Adriano Alonso Veloso, and Frederico Gadelha Guimaraes. Causal graph fuzzy llms: A first introduction and applications in time series forecasting, 2025. URL <https://arxiv.org/abs/2507.17016>.
- Jonas Peters, Dominik Janzing, and Bernhard Schölkopf. Causal inference on time series using restricted structural equation models. *Advances in neural information processing systems*, 26, 2013.
- Jakob Runge. Discovering contemporaneous and lagged causal relations in autocorrelated nonlinear time series datasets. 124:1388–1397, 2020.
- Xinlei Wang, Maike Feng, Jing Qiu, Jinjin Gu, and Junhua Zhao. From news to forecast: integrating event analysis in llm-based time series forecasting with reflection. NIPS '24, Red Hook, NY, USA, 2025. Curran Associates Inc. ISBN 9798331314385.
- Shuhei Watanabe. Tree-structured parzen estimator: Understanding its algorithm components and their roles for better empirical performance. 2023. URL <https://arxiv.org/abs/2304.11127>.

## Appendix A. Experimental Setup and Methodological Details

### A.1. PySIRTEM Epidemic Simulator

PySIRTEM (Biswas et al., 2025) is an extended *Susceptible-Expected-Infected-Recovered* (SEIR) model that uses Delay Differential Equations (DDEs) with compartments that represent, in addition

to the original SEIR ones, health processes such as hospitalization, immunity, and testing. A complete list of transition parameters can be found in (Azad et al., 2022). Without loss of generality, this work uses PySIRTEM as the basis to show the proposed explanation-generation approach. In fact, ruleXplain is independent from PySIRTEM, but a simulator is needed in the evaluation loop (see Fig. 1).

With PySIRTEM as base simulator, to demonstrate ruleXplain, we focus on generating explanations for two timeseries, the *symptomatic testing rate* ( $X_s = \Phi_s = (x_{s,1}, x_{s,2}, x_{s,3}, \dots, x_{s,T})$ ) and the *asymptomatic testing rate* ( $X_a = \Phi_a = (x_{a,1}, x_{a,2}, x_{a,3}, \dots, x_{a,T})$ ), where  $x_{s,t}$  and  $x_{a,t}$  represent the daily ratio of the symptomatic and asymptomatic population tested against the total population for day  $t$ , respectively. The pair  $\{(X_s, X_a)\}_t$  can be modeled as a discrete time timeseries. These timeseries are important to understand the daily infected population (output timeseries) and they can be implemented as decisions (e.g., from the local government). Following the PySIRTEM notation and the modeling introduced in Biswas et al. (2025), the following holds:

$$Y_t = I_t = r \cdot (PS_t + PA_t + IA_t + ATN_t) + IS_t + STN_t. \quad (4)$$

In eqn. (4),  $PS$  and  $PA$  are the pre-symptomatic and pre-asymptomatic population,  $IS$  and  $IA$  are the symptomatic and asymptomatic infected population, and  $ATN$  and  $STN$  are Asymptomatic and Symptomatic population who test negative (by error), respectively. The quantity  $r$  is the ratio between transmission rates for the asymptomatic against symptomatic population.  $PS, PA, IS, IA, STN$ , and  $ATN$  are represented in PySIRTEM as compartments and they are directly affected by the timeseries  $X_s$  and  $X_a$ . In this work, we treat PySIRTEM as a black box system keeping all hyperparameters constant except the timeseries  $X_s$  and  $X_a$ , which ruleXplain will produce as a prediction and explanation for the output timeseries  $Y_t$ . Namely, the relevant input-output pair for the causal inference analysis step of ruleXplain are  $\{(X_s, X_a), Y\}$  where  $X_s$  and  $X_a$  are daily testing rates timeseries (symptomatic and asymptomatic, respectively) and  $Y$  is the list of corresponding daily number of currently infected individuals. In this paper, we consider a simulation horizon of  $T = 100$  days, i.e.,  $t = 1, 2, \dots, T$ , and to maintain the assumptions in PySIRTEM original work, we allow the timeseries for the test rates to only vary weekly, i.e., we impose the test rates to be stepwise constant functions.

ruleXplain uses the PySIRTEM module in two ways: (i) as a learning module (step 1 in Fig. 1) to derive the baseline current daily infected cases  $I_{base}$  from historical data, and secondly as a simulator (step 6 in Fig. 1) to evaluate the effects of the timeseries inputs  $(\Phi_s, \Phi_a)$ . In this work, we refer to  $\Phi_s, \Phi_a$ , and  $I$  as  $X_s, X_a$ , and  $Y$  respectively to avoid domain-specific notations.

## A.2. EnergyPlus Building Energy Simulator

EnergyPlus (Crawley et al., 2001) is a physics-based building energy simulation tool that models building thermal dynamics, HVAC operation, internal loads, and environmental interactions using heat balance equations and system-level energy models. The simulator takes as input a building configuration file (IDF: *Input Data File*) and a weather file (EPW: *EnergyPlus Weather file*). The IDF file specifies the building geometry, dimensions, geological location, materials, HVAC systems, occupancy schedules, and other internal parameters. The IDF also contains the specifications for the run period, variables of interest, and frequency of reporting. The EPW file provides temporal weather data including dry-bulb temperature, solar radiation, humidity, wind speed, and other meteorological variables. EnergyPlus can operate at any temporal resolution. In our experiments, we use hourly simulation outputs.

EnergyPlus can model a wide range of outputs, including zone temperatures, heating and cooling loads, HVAC energy consumption, and total building electricity usage. Without loss of generality, we use EnergyPlus as a second simulation environment to demonstrate the domain-independence of `ruleXplain`. Similar to `PySIRTEM`, `ruleXplain` treats EnergyPlus strictly as a black-box forward simulator within the evaluation loop (see Fig. 1).

For the experiments in this work, we use the *Supermarket* reference building IDF model provided within the standard EnergyPlus example files. As weather input, we use the file `USA_VA_Sterling-Washington-Dulles.Intl.AP.epw` from the official EnergyPlus weather database. The simulation horizon is set to 100 consecutive hours and the baseline data is from Jan 1 to Jan 5, 1997. The relevant input–output pair for the causal analysis step of `ruleXplain` is

$$\{(X_d, X_g), Y\},$$

where:

- $X_d$  denotes outdoor dry-bulb temperature (in °C),
- $X_g$  denotes global horizontal irradiance (in Wh/m<sup>2</sup>),
- $Y$  denotes total building electricity consumption (in J).

Outdoor dry-bulb temperature represents ambient air temperature affecting heat transfer across the building and Global horizontal irradiance measures the total solar radiation incident on a horizontal surface, influencing solar heat gains through windows and building surfaces. Both variables directly affect cooling loads and HVAC operation and impact electricity consumption which is our output variable of interest.

In this work, we observe temperature and irradiance as multivariate input trajectories  $X_t$ , while keeping all building physical properties and HVAC parameters fixed. The simulator maps these environmental inputs to hourly electricity consumption  $Y$ .

`ruleXplain` uses the EnergyPlus module analogously to the epidemic case: (i) to generate a baseline electricity consumption trajectory  $Y_{\text{base}}$  under reference weather conditions, and (ii) to evaluate candidate multivariate input trajectories during rule refinement. As before, we abstract the domain-specific notation and refer to temperature, irradiance, and electricity consumption as  $X_d$ ,  $X_g$ , and  $Y$ , respectively, to maintain consistency across domains.

### A.3. Dimensionality Reduction and Clustering

To reduce redundancy and extract representative data points that will form the training set for the explanation generation step (Sec. 2.3), we apply dimensionality reduction and clustering on the set of timeseries resulting from the input timeseries learning step (Sec. 2.1),  $\{(X_s^p, X_a^p)\}_{p=1}^N$ .

**Dimensionality reduction.** As each candidate comprises of two daily timeseries vectors,  $X_s = (x_{s,1}, x_{s,2}, \dots, x_{s,T})$  and  $X_a = (x_{a,1}, x_{a,2}, \dots, x_{a,T})$ , the input space is  $2T$ -dimensional. Because of the high-dimensionality and non-linearity of the input space, we first reduce the dimensionality considering only the weekly changing points (this is not necessary to the application of the framework), and, on the reduced dimensionality timeseries, we employ the Uniform Manifold Approximation and Projection (UMAP) (McInnes et al., 2020) technique to represent the data points in a 2-D space embedding for clustering. UMAP facilitates visual confirmation of cluster separability by constructing a high-dimensional topological representation of the data and then optimizing a

low-dimensional graph to be as structurally similar as possible through cross-entropy minimization. Unlike other linear (Principle Component Analysis or PCA) and non-linear techniques (t-distributed Stochastic Neighbor Embedding or t-SNE), UMAP preserves both local and global structure with competitive accuracy (McInnes et al., 2020).

**Clustering the reduced-dimensionality timeseries.** Upon reduction to a 2-D input space, we employ a  $K$ -Means clustering to identify distinct input timeseries “trends”. We choose  $K$ -Means clustering due to its simplicity and efficiency in detecting separable clusters. The input timeseries corresponding with the centroids of each cluster are represented by  $(X_s^c, X_a^c)$ . As all  $(X_s^c, X_a^c)$  result in output trends identical to  $Y_{base}$ , we denote the input-output pairs of each clusters as  $((X_s^c, X_a^c), Y_{base})$  for simplicity.

The primary purpose of clustering in `ruleXplain` is to elect a single representative data point from each solution cluster as inducing timeseries within the training set during the LLM phase (see Sec. 2.3). We argue that such data reduction can help in the training context emphasizing diversity, removing redundant examples that may result into overly “engineered” explanations (rulesets  $\mathcal{R}$ ), while removing the influence of individual cluster size or density. Since all the input pairs generate the same output trajectory ( $Y_{base}$ ), we argue that a diverse training set facilitates the LLM task to extrapolate the implicit, causal relation between the variables.

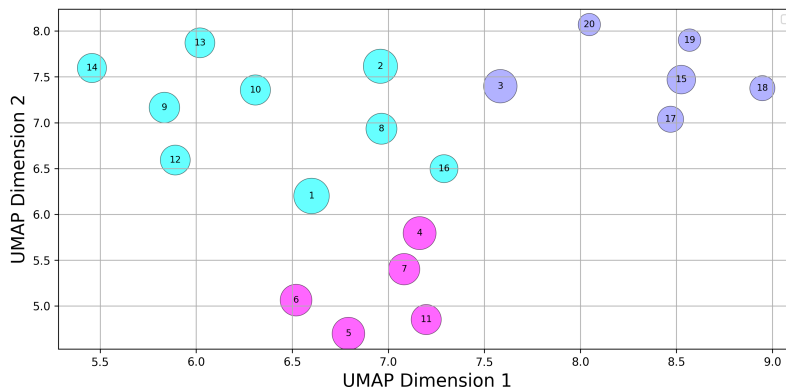


Figure 7: Clustering of the initial solution pool  $\{(X_s^p, X_a^p)\}_p$  from solving  $P_{LEARN}(p)$  for `PYSIRTEM` setup.

## Appendix B. Extended Results and Analysis

In this section, we report the final extracted ruleset after the closed-loop refinement process of `ruleXplain` for both `PYSIRTEM` (Table. 2) and `EnergyPlus` (Table 3).

Figure 8 reports the iterative reconstruction loss produced by the closed-loop pipeline. At each iteration, a symbolic ruleset is extracted or refined, the LLM is prompted to generate input trajectories consistent with the rules, and the simulator is executed to obtain  $Y_{sim}$ . The output loss  $L_{out}(Y_{sim}, Y_{base})$ —measured as Mean Squared and Normalized Mean Squared Difference—is then computed. The decreasing trend observed for both (a) `PYSIRTEM` and (b) `EnergyPlus` demonstrates that successive rule refinements generate inputs whose simulated outputs progressively align

Table 2: Causal rules extracted from timeseries examples and context for PySIRTEM Setup.

Rule ID	Input Window	$X_s$ Trend	$X_a$ Trend	Output Window	Y Phase	Symbolic Rule
R1	[0, 14]	Low	SlowRise	[15, 29]	InitialGrowth	$\square_{[0,14]}(\text{Low}(X_s) \wedge \text{SlowRise}(X_a)) \rightarrow \diamond_{[15,29]}\text{InitialGrowth}(Y)$
R2	[14, 28]	Moderate	SlowRise	[29, 43]	PeakFormation	$\square_{[14,28]}(\text{Moderate}(X_s) \wedge \text{SlowRise}(X_a)) \rightarrow \diamond_{[29,43]}\text{PeakFormation}(Y)$
R3	[28, 42]	SharpSpike	Low	[43, 57]	PostPeak	$\square_{[28,42]}(\text{SharpSpike}(X_s) \wedge \text{Low}(X_a)) \rightarrow \diamond_{[43,57]}\text{PostPeak}(Y)$
R4	[42, 56]	DipThenRise	Low	[57, 71]	Decline	$\square_{[42,56]}(\text{DipThenRise}(X_s) \wedge \text{Low}(X_a)) \rightarrow \diamond_{[57,71]}\text{Decline}(Y)$
R5	[56, 70]	SlowRise	HighStable	[71, 85]	Resurgence	$\square_{[56,70]}(\text{SlowRise}(X_s) \wedge \text{HighStable}(X_a)) \rightarrow \diamond_{[71,85]}\text{Resurgence}(Y)$
R6	[70, 100]	Moderate	SlowRise	[85, 100]	PeakFormation	$\square_{[70,100]}(\text{Moderate}(X_s) \wedge \text{SlowRise}(X_a)) \rightarrow \diamond_{[85,100]}\text{PeakFormation}(Y)$

Table 3: Causal rules extracted from timeseries examples and context for EnergyPlus Setup.

Rule ID	Input Window	$X_{t,1}$ Trend	$X_{t,2}$ Trend	Output Window	Y Phase	Symbolic Rule
R1	[0, 9]	Low	Low	[0, 8]	Decline	$\square_{[0,9]}(\text{Low}(X_{t,1}) \wedge \text{Low}(X_{t,2})) \rightarrow \diamond_{[0,8]}\text{Decline}(Y)$
R2	[9, 18]	SlowRise	SharpSpike	[9, 17]	InitialGrowth	$\square_{[9,18]}(\text{SlowRise}(X_{t,1}) \wedge \text{SharpSpike}(X_{t,2})) \rightarrow \diamond_{[9,17]}\text{InitialGrowth}(Y)$
R3	[18, 21]	DipThenRise	LowModerate	[18, 20]	PostPeak	$\square_{[18,21]}(\text{DipThenRise}(X_{t,1}) \wedge \text{LowModerate}(X_{t,2})) \rightarrow \diamond_{[18,20]}\text{PostPeak}(Y)$
R4	[21, 30]	Low	Low	[21, 29]	Decline	$\square_{[21,30]}(\text{Low}(X_{t,1}) \wedge \text{Low}(X_{t,2})) \rightarrow \diamond_{[21,29]}\text{Decline}(Y)$
R5	[30, 42]	Moderate	HighStable	[30, 41]	PeakFormation	$\square_{[30,42]}(\text{Moderate}(X_{t,1}) \wedge \text{HighStable}(X_{t,2})) \rightarrow \diamond_{[30,41]}\text{PeakFormation}(Y)$
R6	[42, 48]	DipThenRise	LowModerate	[42, 47]	PostPeak	$\square_{[42,48]}(\text{DipThenRise}(X_{t,1}) \wedge \text{LowModerate}(X_{t,2})) \rightarrow \diamond_{[42,47]}\text{PostPeak}(Y)$
R7	[48, 54]	Low	Low	[48, 53]	Decline	$\square_{[48,54]}(\text{Low}(X_{t,1}) \wedge \text{Low}(X_{t,2})) \rightarrow \diamond_{[48,53]}\text{Decline}(Y)$
R8	[54, 66]	Moderate	HighStable	[54, 65]	PeakFormation	$\square_{[54,66]}(\text{Moderate}(X_{t,1}) \wedge \text{HighStable}(X_{t,2})) \rightarrow \diamond_{[54,65]}\text{PeakFormation}(Y)$
R9	[66, 72]	DipThenRise	LowModerate	[66, 71]	PostPeak	$\square_{[66,72]}(\text{DipThenRise}(X_{t,1}) \wedge \text{LowModerate}(X_{t,2})) \rightarrow \diamond_{[66,71]}\text{PostPeak}(Y)$
R10	[72, 78]	Low	Low	[72, 77]	Decline	$\square_{[72,78]}(\text{Low}(X_{t,1}) \wedge \text{Low}(X_{t,2})) \rightarrow \diamond_{[72,77]}\text{Decline}(Y)$
R11	[78, 90]	SlowRise	HighStable	[78, 89]	Resurgence	$\square_{[78,90]}(\text{SlowRise}(X_{t,1}) \wedge \text{HighStable}(X_{t,2})) \rightarrow \diamond_{[78,89]}\text{Resurgence}(Y)$
R12	[90, 96]	DipThenRise	LowModerate	[90, 95]	PostPeak	$\square_{[90,96]}(\text{DipThenRise}(X_{t,1}) \wedge \text{LowModerate}(X_{t,2})) \rightarrow \diamond_{[90,95]}\text{PostPeak}(Y)$
R13	[96, 102]	Low	Low	[96, 100]	Decline	$\square_{[96,102]}(\text{Low}(X_{t,1}) \wedge \text{Low}(X_{t,2})) \rightarrow \diamond_{[96,100]}\text{Decline}(Y)$

with the baseline trajectory, highlighting the effectiveness of the iterative refinement–verification process.

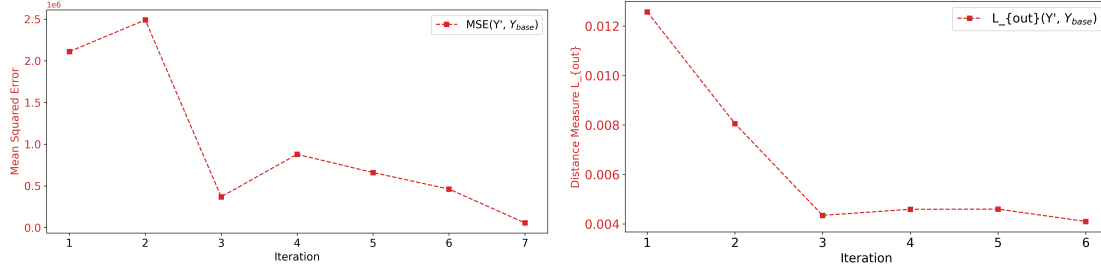


Figure 8: ruleXplain input timeseries produced Mean Squared Difference across iterations for (left) PySIRTEM (right) EnergyPlus

## Appendix C. Detailed Prompts for LLM

The codebase used during the course of this work can be found [here](#).

### C.1. ruleXplain Framework Prompts

The following prompts are used during ruleXplain’s LLM-based Explanation Generation (Sec. 2.3):

- 1. Initial Explanation Inference Prompt.** This prompt provides the LLM with cluster-derived contexts and asks to generate an interpretable, formal ruleset describing input-output relations (Fig. 9).
- 2. Input set generation using ruleset.** This prompt instructs the LLM to use the provided ruleset and cluster-derived context to generate a novel input series (Fig. 10).
- 3. Ruleset refinement prompt.** This provides the LLM with the simulated output  $Y'$  resulting from the generated  $(X'_s, X'_a)$  and  $Y_{base}$  along with the previously available contexts. The LLM is then asked to assess the deviations of  $Y'$  and  $Y_{base}$  and refine the ruleset (Fig. 11).

### C.2. Validation Experiment Prompts

The following prompts have been used to validate ruleXplain:

- 1. (S1) Executing LLM with no rules and no cluster-derived context (Sec. 3.3).** we provide the LLM with only the target output  $Y_{base}$ , existence of causal dependency between inputs and outputs, and the valid input ranges. The LLM is further instructed to avoid any domain specific knowledge (Fig 12).
- 2. (E2) Input generation with inaccurate ruleset.** We modify the ruleset by inverting and replacing a subset of the input-output timeseries relationships. This produces an **inaccurate** ruleset  $\mathcal{R}_{incorrect}$  (Table 4), and we want to observe how the inaccuracy of rules affects the generation of the input timeseries and, consequently, the alignment between  $Y_{incorrect}$  and  $Y_{base}$ . We use the inaccurate ruleset in the same prompt as Fig. 10.

**Goal: Generate initial causal rules  $R_0$  from clustering context**

**Prompt:**

You are given several input-output examples from a timeseries simulation model. Each example consists of a multivariate input timeseries  $X_t$  and a univariate daily output timeseries  $Y$ .

The input  $X_t$  is defined over a time interval length  $\{\Delta\}$ . If  $Y$  spans 100 days, then  $X_t$  will contain  $\lceil 100/\Delta \rceil$  interval values. The relationship between inputs and outputs is be  $\{\text{direct/inverse}\}$  and may include temporal lag/delay effects.

Your goal is to observe the input-output relationships from the examples and extract symbolic causal rules of the form:

“If trends in selected components of  $X_t$  persist over a given time interval, then the output  $Y$  will exhibit a specific phase after a delay.”

Please divide the baseline output into specific output phases listed below in order of timing and infer the multivariate input trends that are responsible. Each output phase should be unique (no duplicate entries in the output column), and the rules should provide input and corresponding output trend behavior for the total time window (i.e., all input windows should concatenate to cover from  $T = 0$  to  $T = 100$ ). Input time windows must be multiples of  $\Delta$ .

Fill in the table below with symbolic causal rules. Each rule should specify:

- Input Trend Window: the time interval where a specific trend in selected components of  $X_t$  is observed.
- Trend Description: qualitative trends over that window.
- Output Phase Window: the time interval where a specific phase in  $Y$  occurs, as a delayed effect of the input.
- Phase Description: the qualitative behavior of  $Y$ .
- Symbolic Rule: a formal statement capturing this as a logical implication.

Use the vocabulary:

- Trends: Low, Moderate, HighStable, SharpSpike, SlowRise, DipThenRise, LowModerate
- Output Phases: InitialGrowth, PeakFormation, PostPeak, Decline, Resurgence

Below is the list of example input-output points and Baseline Expected Output:

— Example 0 —

$X_{t,1}$ : [0.018, 0.14, ...  $K$  values],  $X_{t,2}$ : [0.06, 0.23, ...  $K$  values],  $Y$ : [15, 12, ...  $T$  values]

— Example 1 —

$X_{t,1}$ : [0.025, 0.083, ...  $K$  values],  $X_{t,2}$ : [0.05, 0.19, ...  $K$  values],  $Y$ : [15, 12, ...  $T$  values]

{Insert More ...}

Baseline  $Y$ : [15, 12, ...  $T$  values]

Table format:

Rule ID	Input Trend Window	$X_s$ Trend	$X_a$ Trend	Output Phase Window	$Y$ Phase	Symbolic Rule
R1	[0, 15]	Low	SlowRise	[0, 20]	PeakFormation	$\square_{[0,15]}(\text{Low}(X_s) \wedge \text{SlowRise}(X_a)) \rightarrow \diamond_{[0,20]}\text{PeakFormation}(Y)$
R2	[15, 30]	Low	Low	[20, 35]	InitialGrowth	$\square_{[15,30]}(\text{Low}(X_s) \wedge \text{Low}(X_a)) \rightarrow \diamond_{[20,35]}\text{InitialGrowth}(Y)$

Make sure to use the table format shown above. Do not use domain-specific terminology; instead, describe timeseries patterns using abstract trend labels. Ensure the symbolic rule column uses the logical form:

$$\square_{[t_1,t_2]}(\text{Trend}(X_{t,i}) \wedge \text{Trend}(X_{t,j}) \wedge \dots) \rightarrow \diamond_{[t_3,t_4]}\text{Phase}(Y)$$

Ensure:

- All time windows are valid.
- Input windows are multiples of  $\Delta$ .
- Output phases are unique and cover the full timeline.
- The symbolic rule strictly follows the required logical template.
- Only abstract trend labels are used.

Figure 9: Prompt for generating the initial ruleset.

Table 4: Inaccurate Causal Rules used for Input Generation for Generalizability Experiment for PySIRTEM

Rule ID	Input Window	$X_{t,1}$ Trend	$X_{t,2}$ Trend	Output Window	Y Phase	Symbolic Rule
R1	[0, 14]	SharpSpike	Low	[15, 29]	InitialGrowth	$\Box_{[0,14]}(\text{SharpSpike}(X_s) \wedge \text{Low}(X_a)) \rightarrow$ $\Diamond_{[15,29]}\text{InitialGrowth}(Y)$
R2	[14, 28]	HighStable	HighStable	[29, 43]	PeakFormation	$\Box_{[14,28]}(\text{HighStable}(X_s) \wedge$ $\text{HighStable}(X_a)) \rightarrow$ $\Diamond_{[29,43]}\text{PeakFormation}(Y)$
R3	[28, 42]	Low	DipThenRise	[43, 57]	PostPeak	$\Box_{[28,42]}(\text{Low}(X_s)$ $\text{DipThenRise}(X_a)) \rightarrow$ $\Diamond_{[43,57]}\text{PostPeak}(Y)$
R4	[42, 56]	SharpSpike	HighStable	[57, 71]	Decline	$\Box_{[42,56]}(\text{SharpSpike}(X_s)$ $\text{HighStable}(X_a)) \rightarrow$ $\Diamond_{[57,71]}\text{Decline}(Y)$
R5	[56, 70]	Moderate	Low	[71, 85]	Resurgence	$\Box_{[56,70]}(\text{Moderate}(X_s) \wedge \text{Low}(X_a)) \rightarrow$ $\Diamond_{[71,85]}\text{Resurgence}(Y)$
R6	[70, 100]	HighStable	HighStable	[85, 100]	PeakFormation	$\Box_{[70,100]}(\text{HighStable}(X_s)$ $\text{HighStable}(X_a)) \rightarrow$ $\Diamond_{[85,100]}\text{PeakFormation}(Y)$

**Goal: Novel input set  $(X'_s, X'_a)$  generation using ruleset  $\mathcal{R}_i$**

**Prompt:** You are given several input-output examples from a timeseries simulation model and a causal ruleset describing input trends and their corresponding output effects.  
 Each example consists of:

- A multivariate input timeseries  $X_t$  defined over interval length  $\Delta$
- A daily output timeseries  $Y$

All example inputs generate the same output  $Y$ . The relationship between inputs and outputs is direct and may include temporal lag/delay effects. The baseline output  $Y$  spans 100 days. The input  $X_t$  is defined over interval length  $\{\Delta\}$ , so  $X_t$  contains  $\lceil 100/\Delta \rceil$  interval values.

Input constraints:

- All  $X_{t,1}$  values must lie in the range  $\{Insert\ Range\}$
- All  $X_{t,2}$  values must lie in the range  $\{Insert\ Range\}$

You must use the provided ruleset to generate a novel multivariate input sequence  $X_t$  that is different from all example inputs but produces an output  $Y$  that closely follows the baseline  $Y$  trend.

**Instructions:**

1. Analyze the baseline  $Y$  trend and the provided ruleset.
2. Divide the baseline  $Y$  into output phases.
3. For each output phase:
  - Identify the corresponding rule in the ruleset.
  - Determine the required input trends.
4. Generate a new multivariate input sequence  $X_t$ :
  - Length must match the number of intervals determined by  $\Delta$ .
  - Trends must be consistent with the ruleset.
  - The full timeline must be covered.
  - The trend pattern must differ from all previous example inputs.
  - All input values must satisfy the specified bounds.
5. For each output phase, briefly justify your input choices for the corresponding input intervals, referencing:
  - The applied rule
  - The delayed and direct relationship between inputs and output

Below is the list of example input-output points and Baseline Expected Output:  
 $\{Insert\ Clustering\ Context\ \dots\}$

---

Baseline  $Y$ :  $\{Baseline\ Output\}$   
 Rules Table:  $\langle Insert\ Ruleset\ in\ Markdown\ format \rangle$

**Required Output Format:**

1. **Generated Input Series:** Provide the full multivariate input sequence:  
 -  $X_{t,1}$ :  $[v_1, v_2, \dots, v_K]$ ,  $X_{t,2}$ :  $[v_1, v_2, \dots, v_K], \dots$
2. **Phase-wise Justification:** For each output phase, provide:  
**Output Phase:** PhaseName, **Output Window:**  $[t_3, t_4]$ , **Applied Rule:** RuleID, **Required Input Trend Window:**  $[t_1, t_2]$ , **Assigned Input Trends:**  $X_{t,i}$ : Trend  
**Justification:** Brief explanation referencing the rule and the delayed/direct or inverse relationship.

Ensure:

- The generated input trends differ structurally from all example inputs.
- Input intervals are multiples of  $\Delta$ .
- The ruleset is followed consistently.
- The entire timeline is covered.
- All input values lie within the specified range.
- The resulting  $Y$  closely follows the baseline  $Y$ .

Figure 10: Prompt for Novel Input series generation using inferred ruleset  $\mathcal{R}_i$ .

**Goal: Ruleset Refinement by evaluating  $Y'$  (generated from  $(X'_s, X'_a)$  and  $Y'_{base}$ )**

**Prompt:**

You previously generated a multivariate input series  $X'_t$  using a causal ruleset, simulated the system, and obtained an output  $Y'$ . The simulated output  $Y'$  does not closely match the Baseline  $Y$ . The relationship between inputs and output is {direct/inverse} and delayed. This is critical and must guide your diagnosis and rule updates.

**Generated Input:**

$X'_t$ : Your generated weekly input timeseries:  
 $\{Insert X_{t,sim}\}$   
 corresponding  $Y'$ :  $\{Insert Y_{sim}\}$

Baseline  $Y$ :  $\{Insert Y_{base}\}$   
 Previous Rules Table:  $\langle Insert Ruleset in Markdown Format \rangle$

**Instructions:**

1. Divide the Baseline  $Y$  into distinct output phases in chronological order.
2. Compare  $Y'$  with Baseline  $Y$  and identify mismatches, including: Timing shifts, magnitude differences, shape differences (peaks, valleys, slopes), and phase misalignment.
3. Diagnose which input trends in  $X'_t$  caused the mismatch, considering whether they were too high or too low, too early or too late, too sharp or too flat, not sustained long enough, or incorrectly capturing the direct or delayed relationship.
4. Update the ruleset to better guide future input generation.

**Constraints for Updated Rules:**

Each output phase must be unique.  
 Input windows must be multiples of  $\Delta$ .  
 Input windows must concatenate to cover the full timeline ( $T = 0$  to  $T = 100$ ).  
 Use only abstract trend labels.  
 Do not use domain-specific terminology.  
 When appropriate, refine only the input variable most responsible for a mismatch.

**Allowed Vocabulary:**

Input Trends: Low, Moderate, HighStable, SharpSpike, SlowRise, DipThenRise, LowModerate  
 Output Phases: InitialGrowth, PeakFormation, PostPeak, Decline, Resurgence

**Required Output Format:**  
 Return the updated rules in following Markdown table format:

Rule ID	Input Trend Window	$X_s$ Trend	$X_a$ Trend	Output Phase Window	Y Phase	Symbolic Rule
R1	[t1,t2]	Low	SlowRise	[t3,t4]	PeakFormation	$\square_{[t1,t2]}(\text{Low}(X_{t,1}) \wedge \text{SlowRise}(X_{t,2})) \rightarrow \diamond_{[t3,t4]}\text{PeakFormation}(Y)$

**Symbolic Rule Format:**

Each rule must follow:

$$\square_{[t1,t2]}(\text{Trend}(X_{t,i}) \wedge \text{Trend}(X_{t,j}) \wedge \dots) \rightarrow \diamond_{[t3,t4]}\text{Phase}(Y)$$

Ensure: Rules better explain the mismatch between  $Y'$  and Baseline  $Y$ . The direct and delayed relationship must be properly encoded. The updated rules should improve future alignment with Baseline  $Y$ .

Figure 11: Prompt for Ruleset Refinement.

**Goal: Novel Input Generation without Rules or Context****Prompt:**

You are given a system that takes as input a multivariate timeseries parameters  $X_t$  defined over interval length  $\Delta$ , and produces a daily output timeseries  $Y$ . If  $Y$  spans  $\{T\}$  days, each input sequence contains  $\lceil \{T\}/\{\Delta\} \rceil$  values.

Given a target output trajectory  $Y$  over  $\{T\}$  days and the valid range for each input parameter, your task is to infer a pair of input sequences that could plausibly generate the same output.

Input constraints:

- All  $X_{t,1}$  values must lie within  $\{Insert\ Range_1\}$
- All  $X_{t,2}$  values must lie within  $\{Insert\ Range_2\}$   
 $\{Insert\ More\}$

Do not provide code. Infer the input values directly from the given output pattern. Do not use any domain-specific knowledge; treat the inputs and outputs as abstract functional relationships.

**Required Output Format:**

Provide the full multivariate input sequences explicitly:

$$X_{t,1} = [v_1, v_2, \dots, v_K], \quad X_{t,2} = [v_1, v_2, \dots, v_K].$$

Figure 12: Prompt for Input Generation with **no rules + no clustering context**

